Received: 16 September 2021 | Revised: 21 November 2021 | Accepted: 12 December 2021

DOI: 10.1002/sus2.41

SusMat WILEY

RESEARCH ARTICLE

Precise modification of poly(aryl ether ketone sulfone) proton exchange membranes with positively charged bismuth oxide clusters for high proton conduction performance

Yi-Zhuo Yin[1] | **Zhen-Guo Zhang**[2] | **Wen-Wen He**[1] | **Jing-Mei Xu**[2] | **Feng-Yu Jiang**[1] | **Xu Han**[1] | **Wan-Ting Di**[1] | **Zhe Wang**[2] | **Shengqian Ma**[3]

[1] School of Chemistry and Life Science, Advanced Institute of Materials ScienceChangchun University of Technology, Changchun, China

[2] Advanced Institute of Materials ScienceChangchun University of Technology, Changchun, China

[3] Department of Chemistry, University of North Texas, Denton, Texas

Correspondence
Shengqian Ma, Department of Chemistry, University of North Texas, 1508 W. Mulberry St. Denton, TX 76201.
Email: Shengqian.Ma@unt.edu

Yi-Zhuo Yin and Zhen-Guo Zhang contributed equally to this work.

Funding information
National Natural Science Foundation of China, Grant/Award Numbers: 21701016, 51803011; Science and Technology Development Planning of Jilin Province, Grant/Award Number: 20190103129JH; Education Department of Jilin Province, Grant/Award Number: JJKH20200666KJ; China Scholarship Council, Grant/Award Number: 201802335014; Welch Foundation, Grant/Award Number: B-0027

Abstract

In the field of proton exchange membranes (PEMs), it is still a great challenge to explore new Nafion alternatives, maintaining the high proton conductivity and lowering the cost of practical application. In this work, a series of low sulfonated poly(aryl ether ketone sulfone) (SPAEKS) membranes hybridized by $[Bi_6O_5(OH)_3]_2(NO_3)_{10}\cdot 6H_2O$ ($H_6Bi_{12}O_{16}$) have been successfully fabricated. When the doping amount of $H_6Bi_{12}O_{16}$ reaches 5 wt%, the DS15-Bi_{12}-5 showing the best proton conductive ability and mechanical properties. The proton conductivity can achieve 72.8 mS·cm^{-1} at 80°C and the tensile strength can reach 43.57 MPa. Confirmed by experimental data and activation energy (E_a) calculations, the existence of Bi cluster makes more hydrogen bonds, providing additional proton hopping sites and offers more proton transport vehicles, leading to a high proton conduction performance. This work proved that polyoxometalates (POMs) can replace the role of sulfonate groups in SPAEKS to a certain extent and work out the defects of high sulfonation, making a remarkable contribution to the practical application of low sulfonated SPAEKS.

KEYWORDS
polyoxometalates, proton conductivity, proton exchange membrane, sulfonated poly(aryl ether ketone sulfone)

1 | INTRODUCTION

With the aggravation of global energy crisis, it is urgent to develop high efficient energy conversion devices, which meanwhile should be friendly to the environment. Proton exchange membrane fuel cells (PEMFCs) are such promising candidates due to the merits of high efficiency, cleanliness, and sustainability.[1,2] Proton exchange membranes

(PEMs) are the core components of PEMFCs. Perfluorosulfonic acid membrane (PFSA), or Nafion, is the only widely used commercial PEM nowadays. However, many drawbacks such as low water retention capacity when the temperature is above 80°C, significant swelling ratio caused by high degree of sulfonation (DS) and super high cost restrict the large-scale application of PEMFCs.[3a,3b,4,5] So, the exploration of ideal Nafion alternatives has been regarded as the most challenging step in the development of high-performance PEMFCs.

Sulfonated poly(aryl ether ketone sulfone) (SPAEKS) is considered as a promising Nafion substitute owing to its structural designability, simple polymerization process and low-cost characteristics.[6a,6b] The rigid aromatic structure of the main chain makes SPAEKS possessing higher glass transition temperature, good mechanical strength, and excellent thermodynamic stability.[7] SPAEKS with sulfonated main chain is at the forefront of PEMs but poor hydrophilic hydrophobic phase separation severely affects the improvement of proton conduction performance. In recent years, different strategies, such as grafting, cross-linking, and block copolymerization of SPAEKS, have been applied to give outstanding progress of SPAEKS. In 2016, Xu synthesized SPT4 by an amide coupling reaction, 3-amino-1,2,4-triazole was grafted onto C-SPAEKS polymer chain. The proton conductivity of SPT4 reached 0.166 $S{\cdot}cm^{-1}$, 2 times higher than pure C-SPAEKS-3 membrane.[8a] In 2019, Wang prepared cross-linked composite membrane S-Am-2.0/C by cosolvent coating method, exhibiting a proton conductivity of 0.135 $S{\cdot}cm^{-1}$ at 80°C. Besides, S-Am-2.0/C exhibited higher peak power density of 121.09 $mW{\cdot}cm^{-2}$ than that of main-chain type C-SPAEKS membrane (66.65 $mW{\cdot}cm^{-2}$).[8b] In 2020, Lee et al. prepared block copolymer SPAES-LA-X12Y28 with aliphatic chains, which shown a high proton conductivity of 154 $mS{\cdot}cm^{-1}$, achieving power density of 232.02 $mW{\cdot}cm^{-2}$ in H_2/O_2 fuel cell.[8c] However, SPAEKS with high DS usually faced the problems of sharp decline in mechanical properties and over swelling. Therefore, improving the proton conductivity of SPAEKS with low DS is very desirable.[9]

Doping functional inorganic materials to the polymer has been proved to be a promising approach to obtain PEMs with improved proton conduction performance.[10a] In 2020, Sigwadi successfully fabricated Nafion® membrane blended with polyacrylonitrile nanofibers decorated with ZrO_2 and its proton conductivity could achieve 1.84 $S{\cdot}cm^{-1}$ at 25°C.[10b] Furthermore, ionic inorganic fillers can regular the hydrophilic channels and retain water in the SPAEKS matrix, facilitating the conduction of protons.[11–14] In order to take further advantages of additives, enhancing the proton conduction capacity in low DS SPAEKS, a substitute for the sulfonic group is urgently needed. In this way, this strong proton conduction additive can compensate for the loss of proton conduction due to the reduction of sulfonic group; moreover, it can have interactions with the organic part, promoting microphase separation, synergistically increasing the proton conductivity of the whole hybrid system.[15,16]

Polyoxometalates (POMs) are a kind of molecularly well-defined metal-oxide clusters, which have been widely used to prepare hybrid materials due to their high acid strength, dispersity, and thermal stability.[17–20] The main synthetic strategies of POMs included conventional synthesis and hydrothermal method.[21,22] In the past few years, POMs compounds have made excellent achievements in the field of proton conductivity.[23] In 2021, Li's group successfully synthetized a compound of $NaH_{15}\{[P_2W_{15}Nb_3O_{62}]_2(4PBA)_2((4PBA)_2O)\}{\cdot}53H_2O$ reaching high proton conductivity up to 1.59×10^{-1} $S{\cdot}cm^{-1}$ at 90°C.[24] In the same year, Gao obtained a compound of $H_{14}[C_4H_6N_2]_2[Co(H_2O)_5][Co(H_2O)_2]_2\{Co[(PO_3)_3(PO_4)Mo_6O_{15}]_2\}{\cdot}4H_2O$ based on $\{P_4Mo_6\}$; this POM could reach a proton conductivity of 1.33×10^{-2} $S{\cdot}cm^{-1}$ at 75°C.[25] As an excellent potential substitute for sulfonate,[26] advantages of modifying SPAEKS with POMs are: (1) sufficient terminal and bridging oxygen atoms in POMs make their surface an oxygen-rich structure, help to form continuous network of hydrogen bonds, provide vast proton donor and acceptor sites in the process of proton conduction under the Grotthuss mechanism[27]; (2) strong Brönsted acidity makes it possible for POMs to provide protons as a proton source in the form of H^+, H_3O^+, and $H_5O_2^+$, further improving the proton conductivity under the Vehicle mechanism[28]; (3) nanocluster structure of POMs provides the possibility of accurate molecular modification, which can construct molecular-level interactions with monomer units of polymers.[29] In order to solve the solubility problem of POMs in water, electrostatic interactions or acid–base pair needs to be introduced to the host–guest hybrid system preventing leaching of the POMs.[30,31] In 2018, Yoo's group introduced phosphotungstic acid into sulfonated fluorinated block copolymer using facile solution casting approach and the proton conductivity of SFBC-50/PWA-30 can reach 105.22 $mS{\cdot}cm^{-1}$ at 90 °C.[32]

As for the system of SPAEKS, $[Bi_6O_5(OH)_3]_2(NO_3)_{10}{\cdot}6H_2O$ ($H_6Bi_{12}O_{16}$) is an excellent filler candidate not only because of its own good proton conductivity, but also for the high positive charge on the surface of $H_6Bi_{12}O_{16}$ clusters, which can form electrostatic interaction with sulfonate in the main chain. This precise molecular-level hybridization will be conducive to good microphase separation of PEMs, improving the proton conductivity of hybrid membranes. Moreover, bismuth has the characteristics of low toxicity, stable chemical properties, and low price as inorganic fillers; this will make the hybrid PEMs possible for large-scale practical applications. In 2020, Zang's group introduced bismuth

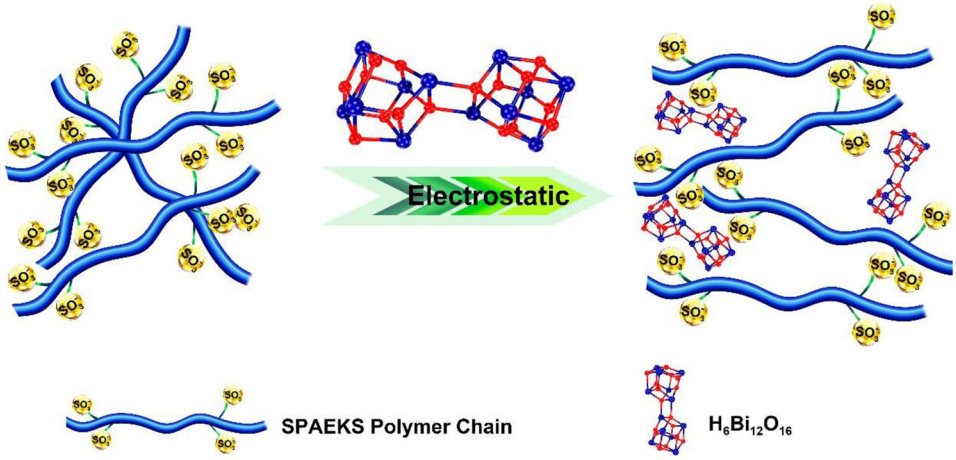

SCHEME 1 Schematic of the hybrid effect of $H_6Bi_{12}O_{16}$ clusters in SPAEKS systems

oxygen clusters into Nafion and successfully obtained Nafion-Bi_{12}-3% with conductivity of 386 mS·cm^{-1} at 80°C and the maximum current density and power density for direct methanol fuel cells reached to 432.7 mA·cm^{-2} and 110.2 mW·cm^{-2}.[33a,33b] It shows that bismuth oxygen cluster has a good hybrid effect on the membrane materials containing sulfonate functional groups.

In this work, we obtained a series of high performance PEMs by hybridizing low-sulfonated SPAEKS (DS 15%) with different amounts of high positive charge $H_6Bi_{12}O_{16}$ (Bi_{12}) clusters (Scheme 1). Study on such a low sulfonation level is very rare. The interaction between the host and guest solves the dissolution problem of the POMs and meanwhile, the existence of Bi_{12} cluster makes more hydrogen bonds, providing additional proton hopping sites and offers more proton transport vehicles, leading to a high proton conduction performance. Specifically, DS15-Bi_{12}-5 (doping amount is 5 wt%) exhibits the best conductivity of 72.8 mS·cm^{-1} at 80°C. Moreover, the tensile strength increased from 37.03 MPa (DS15-Bi_{12}-0) to 43.57 MPa (DS15-Bi_{12}-5); this improvement in mechanical properties makes this hybridization membrane more competitive in practical use. This work proved that POMs can replace the role of sulfonate groups in SPAEKS to a certain extent and work out the defects of high DS, making a remarkable contribution to the practical application of low-sulfonated SPAEKS.

2 | RESULTS AND DISCUSSION

2.1 | Characterization of $H_6Bi_{12}O_{16}$ and hybrid membranes

The structure of $H_6Bi_{12}O_{16}$ was confirmed by powder X-ray diffraction (PXRD), Fourier Transform-Infrared (FT-IR), and TGA. The results were shown in Figure 1. The PXRD curve of as-synthesized $H_6Bi_{12}O_{16}$ was consistent with the simulated one illustrating the cluster has been precisely obtained (Figure 1B). As shown in Figure 1C, the main absorption peaks of $H_6Bi_{12}O_{16}$ were located between 580 cm^{-1} and 1400 cm^{-1}. The strong characteristic absorption peak at 1382 cm^{-1} was attributed to stretching vibration of Bi-O-Bi. It also proved the successful synthesis of the Bi cluster.[33] TGA was performed on as-synthesized $H_6Bi_{12}O_{16}$ to study the thermal stability of this crystal and the TGA curve of $H_6Bi_{12}O_{16}$ was shown in Figure 1D. The weight loss at 109°C can be attributed to the loss of water molecules. And the weight loss appearing at 304 to 570°C was related to the release of nitrate. When the temperature increased above 570°C, the remaining matter was Bi_2O_3.

The chemical structure of SPAEKS was confirmed by ^{1}H NMR (400 MHz, DMSO-d_6). As shown in Figure 2A, the peaks from δ 6.90 to 8.33 ppm were identified as the hydrogen atoms on the benzene ring. The sharp peaks in the range from δ 1.54 to 1.71 ppm were assigned to H of -CH_3 on the side chain, which was consistent with the previous reports.[34] The results of ^{1}H NMR showed that the membrane had been successfully synthesized.

The PXRD pattern of pure SPAEKS (DS15-Bi_{12}-0) matched well with data previously reported (Figure S2). A peak at 6.5° was observed in DS15-Bi_{12}-5 hybrid membrane, which could be attributed to the character peak of $H_6Bi_{12}O_{16}$. The PXRD data proved that $H_6Bi_{12}O_{16}$ had been successfully doped in SPAEKS.

FT-IR spectra of SPAEKS membranes were shown in Figure 2B. The absorption bands at 1230 cm^{-1} and 1078 cm^{-1} could be attributed to the -SO_3H group in the main chain, of which 1230 cm^{-1} was a symmetric O = S = O absorption band and 1078 cm^{-1} was attributed to the asymmetric O = S = O stretching vibration.[34] FT-IR data of the hybrid membranes showed that there was no new peak in

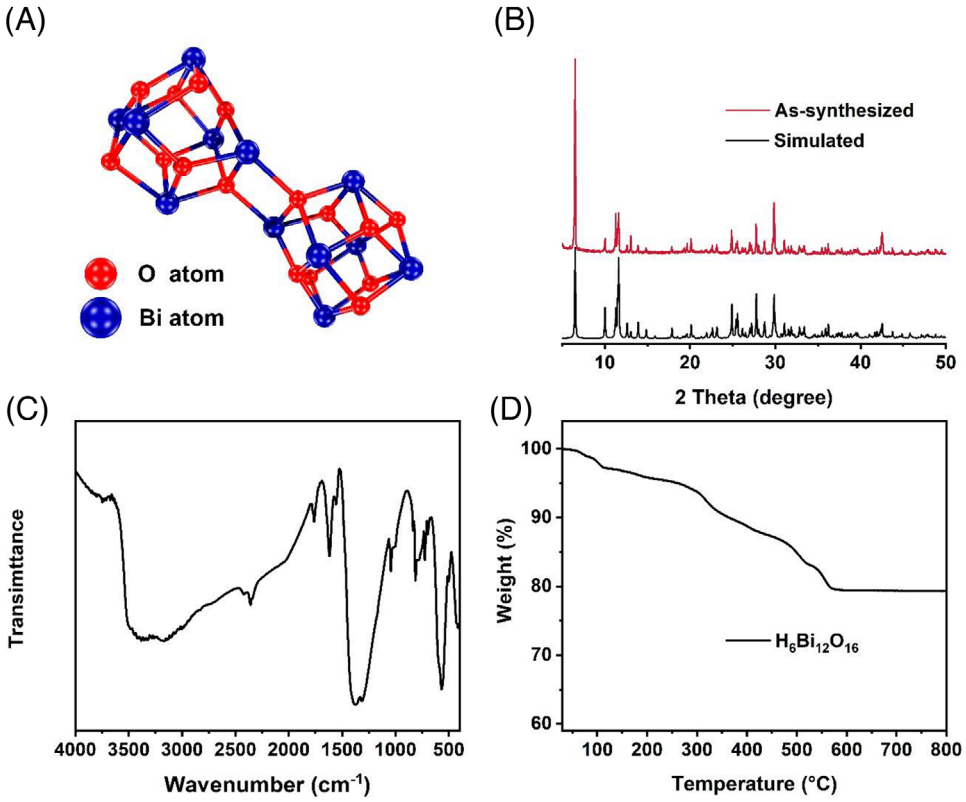

FIGURE 1 (A) Structure of $H_6Bi_{12}O_{16}$; (B) PXRD patterns of $H_6Bi_{12}O_{16}$, as-synthesized sample (red) and simulated one (black); (C) FT-IR spectra of $H_6Bi_{12}O_{16}$, and (D) TGA curve of $H_6Bi_{12}O_{16}$

the hybrid systems instructing introduction of $H_6Bi_{12}O_{16}$ did not change the chemical structure of the membranes.

TGA test was used to analyze the thermal stability of the hybrid membranes. The range of temperature was from 30°C to 800°C with a heating rate of 10°C per minute. Figure 2C shows that there were two main decomposition processes in the undoped SPAEKS membranes: the first gentle weight loss at about 233°C corresponded to the degradation of the sulfonic groups; the second rapid weight loss at about 435°C was attributed to the decomposition of the polymer backbone.

2.2 | Morphology characterizations of the membranes

Because the DS of the hybrid membranes was only 15%, the hybrid membranes were not completely transparent under visible light. In order to observe the influence of $H_6Bi_{12}O_{16}$ doping on the microstructure of the membranes, the cross section of $H_6Bi_{12}O_{16}$-doped hybrid SPAEKS membranes was observed by scanning electron microscope (SEM). The magnification was 7000 times. As shown in Figure 3A, DS15-Bi_{12}-0 had an indeed rough cross section. When the additional amount of $H_6Bi_{12}O_{16}$ reached to 5 wt% (Figure 3B), the cross section of DS15-Bi_{12}-5 became smooth and homogeneous. This uniformity in dispersion may be due to the electrostatic interaction between $H_6Bi_{12}O_{16}$ and sulfonate, and also on account of the strong hydrogen-bond interactions between the polymer matrix and oxygen-rich POMs. However, when the doping amount of $H_6Bi_{12}O_{16}$ reached to 10 wt%, the cross section of DS15-Bi_{12}-10 started to become rough again (Figure 3C). Figure 3D showed that there were obvious agglomerations on the cross section of DS15-Bi_{12}-20, even a small amount of broken crystals appeared, which proved that too much POMs destroyed the compatibility between the host and the guest.

2.3 | Hydrophilicity of the membranes

As water molecules are the carriers of proton, good hydrophilicity is the guarantee of excellent proton conduction performance. Water contact angle test was carried out to directly test the hydrophilic property of membrane materials. As shown in Figure 4, the water contact angle of all $H_6Bi_{12}O_{16}$-doped hybrid SPAEKS membranes were smaller than that of pure SPAEKS membrane DS15-Bi_{12}-0, indicating that the introduction of $H_6Bi_{12}O_{16}$ improved

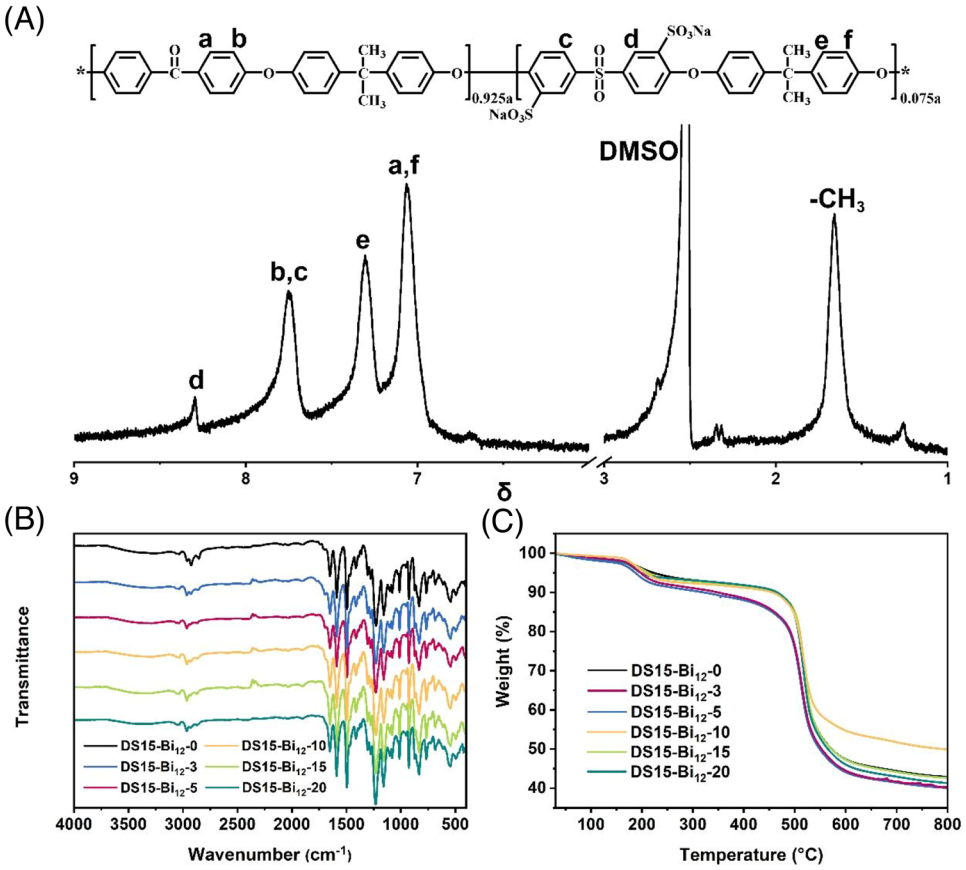

FIGURE 2 (A) ^{1}H NMR of pure SPAEKS; (B) FT-IR spectra, and (C) TGA curves of DS15-Bi_{12}-0 (black curve), DS15-Bi_{12}-3 (blue curve), DS15-Bi_{12}-5 (red curve), DS15-Bi_{12}-10 (yellow curve), DS15-Bi_{12}-15 (light green curve), and DS15-Bi_{12}-20 (dark green curve)

the hydrophilicity of all the hybrid membranes. The water contact angle of the membrane first decreased with the increase of $H_6Bi_{12}O_{16}$ and when the doping amount is 5 wt%, the water contact angle is 69.2°, the smallest one, indicating that the hydrophilic property of DS15-Bi_{12}-5 is the best among all hybrid membranes. And when the content of $H_6Bi_{12}O_{16}$ increased continuously, the hydrophilic property of the membranes decreased.

As shown in Figure 5A, the water uptake values of SPAEKS and all $H_6Bi_{12}O_{16}$-doped hybrid SPAEKS membranes increased with the increasing of temperature. It was obvious that all of the hybrid membranes had a higher water absorption value than pure SPAEKS membrane and the results of water uptake of hybrid membranes showed the same variation law with the previous water contact angle tests. There were amount of new hydrogen interactions in the hybrid system after the incorporation of Bi_{12} clusters. Furthermore, the essential property of POMs itself is also hydrophilic. So the introduction of $H_6Bi_{12}O_{16}$ not only made the hybrid membranes have better hydrophilicity, but also absorb more water molecules. At lower content, this feature played a dominant role with the increase of POMs doping. However, when the doping amount reached to 10 wt%, a downward trend appeared. This may be attributed to that too much fillers occupied the gap between the polymer chains and hindered the movement of polymer chains, leading to a decrease in hydrophilicity and water uptake of the hybrid membranes.

Swelling ratio is a parameter to characterize the dimensional stability of the hybrid membranes. Figure 5B showed the swelling ratio of SPAEKS and $H_6Bi_{12}O_{16}$-doped hybrid SPAEKS membranes. The trend of swelling ratio was consistent with that of water uptake. The swelling ratio of all hybrid membranes at 80°C was less than 10%, showing good dimensional stability. This excellent performance in swelling ratio may be attributed to the low DS of the main chain.

2.4 | Mechanical properties of hybrid membranes

Mechanical property of the membrane is another important factor for the practical use of PEMs. All of the membrane samples were tested by tensile machine and

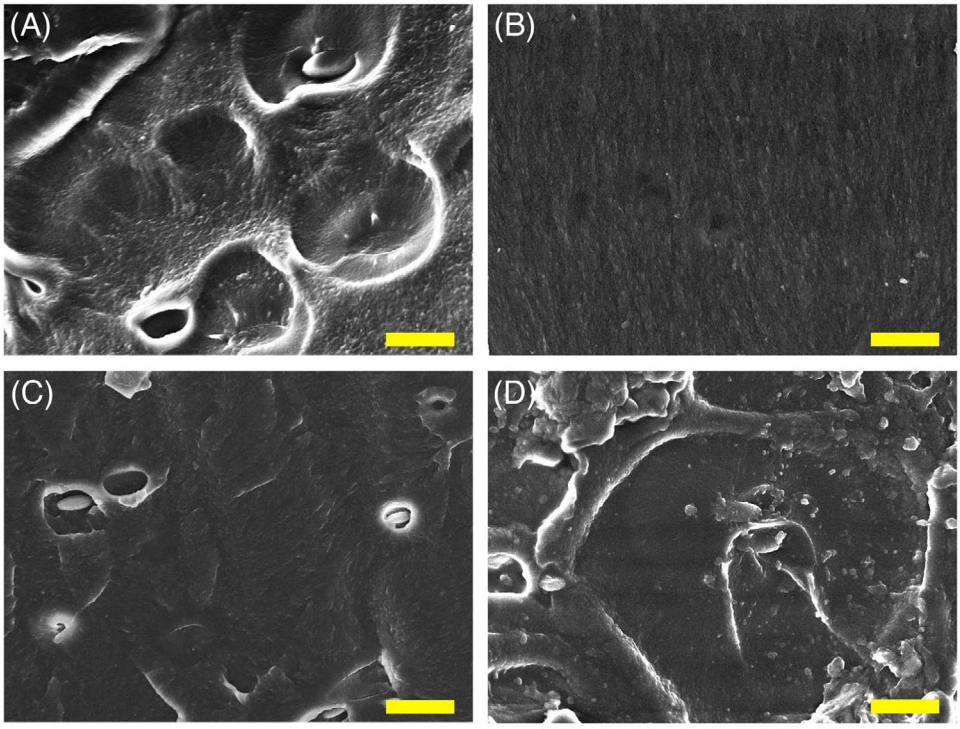

FIGURE 3 SEM images of the cross-section morphology. (A) DS15-Bi_{12}-0; (B) DS15-Bi_{12}-5 (C); DS15-Bi_{12}-10; and (D) DS15-Bi_{12}-20. The magnification is 7000 times and scale bars are 2.5 μm

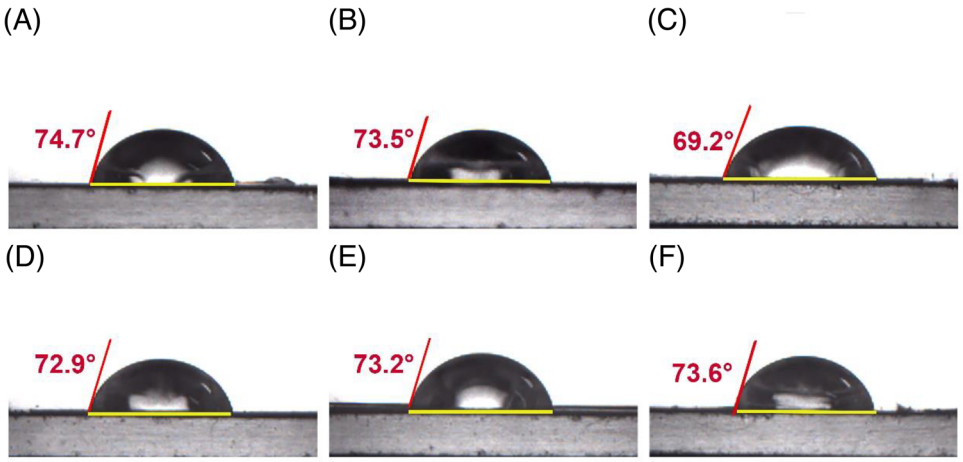

FIGURE 4 Water contact angle of SPAEKS and $H_6Bi_{12}O_{16}$-doped hybrid SPAEKS membranes. (A) DS15-Bi_{12}-0; (B) DS15-Bi_{12}-3; (C) DS15-Bi_{12}-5; (D) DS15-Bi_{12}-10; (E) DS15-Bi_{12}-15; and (F) DS15-Bi_{12}-20

the results were shown in Figure 6 and Table 1. The tensile strength of $H_6Bi_{12}O_{16}$-doped hybrid membranes enhanced with the increase of $H_6Bi_{12}O_{16}$ doping from 0 wt% to 5 wt% (vertical axis of Figure 6). The major reason was the existence of the electrostatic interaction between $H_6Bi_{12}O_{16}$ and sulfonate, and the new hydrogen-bond interactions between the guest cluster and host main chain after the incorporation of Bi clusters, making the microstructure of the hybrid membranes more uniform and orderly, increasing the rigidity. This conjecture was consistent with the characterization results of SEM tests. As the doping amount continued to increase, the tensile strength decreased but the elongation-at-break was visibly enhanced. The over existence of rigid fillers would cause the former decrease. However, it was the increase of Bi clusters that contributed sufficient interactions in the

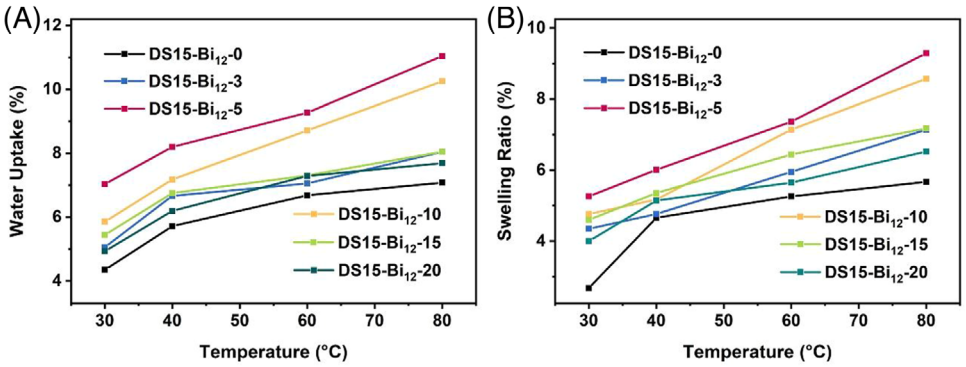

FIGURE 5 Water uptake and swelling ratio of DS15-Bi_{12}-0, DS15-Bi_{12}-3, DS15-Bi_{12}-5, DS15-Bi_{12}-10, DS15-Bi_{12}-15, and DS15-Bi_{12}-20. (A) Water uptake at different temperature. (B) Swelling ratio at different temperature

TABLE 1 Mechanical properties of SPAEKS membrane, $H_6Bi_{12}O_{16}$-doped hybrid SPAEKS membranes and Nafion®212

Sample name	Young's modulus (GPa)	Tensile strength (MPa)	Elongation-at-break (%)
DS15-Bi_{12}-0	1.01 ± 0.0548	37.0 ± 3.30	11.2 ± 0.57
DS15-Bi_{12}-3	1.03 ± 0.0392	39.6 ± 2.44	6.82 ± 1.59
DS15-Bi_{12}-5	1.18 ± 0.0673	43.6 ± 1.92	8.54 ± 1.44
DS15-Bi_{12}-10	1.01 ± 0.0337	37.1 ± 2.93	17.2 ± 1.58
DS15-Bi_{12}-15	1.00 ± 0.0655	35.4 ± 1.78	18.2 ± 2.26
DS15-Bi_{12}-20	0.954 ± 0.0201	39.1 ± 3.35	27.9 ± 3.85
Nafion®212	0.212 ± 0.0689	19.5 ± 0.370	269 ± 9.15

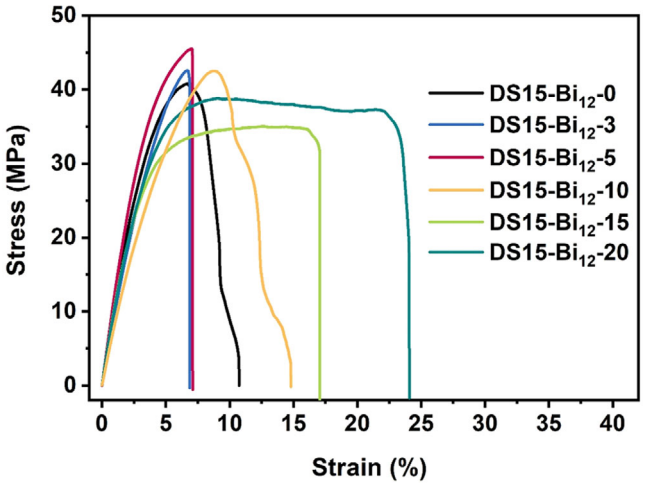

FIGURE 6 Stress–strain curves of DS15-Bi_{12}-0, DS15-Bi_{12}-3, DS15-Bi_{12}-5, DS15-Bi_{12}-10, DS15-Bi_{12}-15, and DS15-Bi_{12}-20

form of chemical bond and hydrogen bond to the toughness of hybrid membranes, leading to an enhanced performance in elongation-at-break values of the hybrid membrane when the amount exceeded 10 wt.% (horizontal axis of Figure 6). In a word, the doping of $H_6Bi_{12}O_{16}$ indeed contributed a lot to the mechanical properties of the membranes, but the way and effect were different.

2.5 | IEC, hydration numbers (λ), and proton conductivity of hybrid membranes

The IEC values of all membrane samples were listed in Table 2. The values of all $H_6Bi_{12}O_{16}$-doped hybrid SPAEKS membranes (0.16–0.38 mmol·g^{-1}) were higher than the pure SPAEKS membrane (0.12 mmol·g^{-1}). Among them, DS15-Bi_{12}-5 has the highest IEC value of 0.38 mmol·g^{-1}, as a result of large number of free protons dissociated from the doped $H_6Bi_{12}O_{16}$ clusters. The hydration numbers (λ) at 30°C of DS15-Bi_{12}-0 to DS15-Bi_{12}-20 were 20.1, 14.0, 10.2, 10.4, 11.6, and 17.1, respectively. λ is the number of water molecules interacted with per sulfonic acid group on polymer structure. In our system, λ decreased with the addition of $H_6Bi_{12}O_{16}$ before 5 wt%, when the doping amount exceed 10 wt%, the data began to increase. This trend may be related to the introduction of POMs. The interaction between Bi_{12} clusters and -SO_3H reaches an optimal state in DS15-Bi_{12}-5; sulfonates were participate in the interaction with $H_6Bi_{12}O_{16}$, reducing the concentration of -SO_3H in the membrane's backbone, leading to a decrease in λ

TABLE 2 Proton conductivity, IEC, and E_a value of SPAEKS membrane and hybrid membranes

Sample name	Proton conductivity ($S \cdot cm^{-1}$) at 30°C	Proton conductivity ($S \cdot cm^{-1}$) at 80°C	IEC ($mmol \cdot g^{-1}$)	E_a ($kJ \cdot mol^{-1}$)
DS15-Bi_{12}-0	1.595×10^{-2}	3.540×10^{-2}	0.12	16.063
DS15-Bi_{12}-3	1.926×10^{-2}	4.436×10^{-2}	0.20	15.957
DS15-Bi_{12}-5	3.031×10^{-2}	7.281×10^{-2}	0.38	15.408
DS15-Bi_{12}-10	2.602×10^{-2}	5.565×10^{-2}	0.32	15.526
DS15-Bi_{12}-15	1.750×10^{-2}	4.571×10^{-2}	0.26	15.742
DS15-Bi_{12}-20	1.780×10^{-2}	4.167×10^{-2}	0.16	15.958

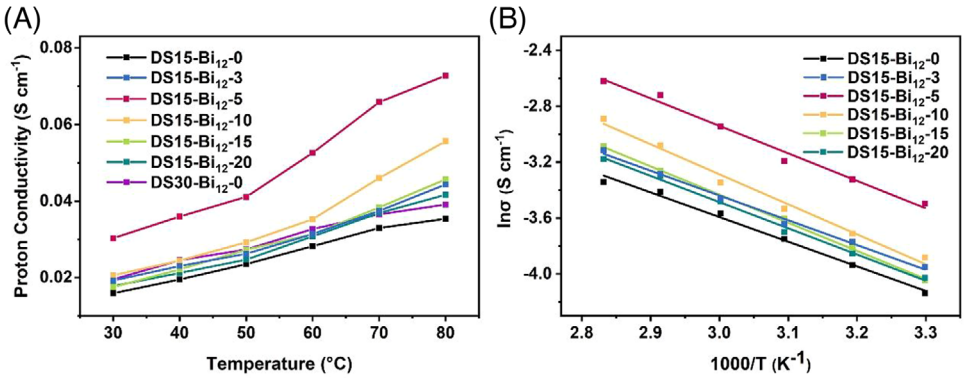

FIGURE 7 Proton conductivity and Arrhenius plot of DS15-Bi_{12}-0, DS15-Bi_{12}-3, DS15-Bi_{12}-5, DS15-Bi_{12}-10, DS_{15}-Bi_{12}-15, and DS15-Bi_{12}-20. (A) Proton conductivity at different temperature. (B) Arrhenius plot at different temperature

value. The proton conductivities were carried out at different temperature. The data showed that the proton conductivities of all membranes increased with the increasing of temperature. It can be observed from Figure 7A that the proton conductivity of all $H_6Bi_{12}O_{16}$-doped hybrid membranes was higher than the pure SPAEKS membrane and increased with the addition of $H_6Bi_{12}O_{16}$, reached the peak when the doping amount was 5 wt%. DS15-Bi_{12}-5 has the highest proton conductivity of 0.0728 $S \cdot cm^{-1}$ at 80°C (0.0303 $S \cdot cm^{-1}$ at 30°C). As the doping amount increased beyond 10 wt%, the conductivity began to decrease. Moreover, the proton conductivity of all hybrid membranes was higher than the pure SPAEKS membrane with DS = 30 at 80°C. This result supported the assumptions that the $H_6Bi_{12}O_{16}$ clusters could be a good substitute for sulfonate in SPAEKS system with low sulfonation degree in proton conduction field.

The Arrhenius plot was shown in Figure 7B. The activation energy (E_a) of pure SPAEKS and $H_6Bi_{12}O_{16}$-doped hybrid SPAEKS membranes was calculated by Arrhenius equation and shown in Table 2. The data revealed that the E_a value of all hybrid membranes was lower than pure SPAEKS membrane and all samples were not higher than 20 $kJ \cdot mol^{-1}$. This result showed that incorporation of Bi clusters reduced the energy barrier and accelerated proton transfer in hybrid PEMs, and Grotthuss mechanism played a leading role in terms of all $H_6Bi_{12}O_{16}$-doped hybrid membranes. The E_a value of DS15-Bi_{12}-5 was 15.048 $kJ \cdot mol^{-1}$, the lowest of all hybrid membranes.

2.6 | Mechanism of proton transport in hybrid membranes

We summarized the improvement in hydrophilic property and proton conductivity of DS15-Bi_{12}-5 as follows: $H_6Bi_{12}O_{16}$ was an oxygen-rich cluster with high proton conductivity. After being incorporated into the SPAEKS membrane, (I) the continuous network of hydrogen bonds between oxygen atoms on the $H_6Bi_{12}O_{16}$ clusters and $-SO_3H$ groups enhanced the water-retention capability and made the hybrid membrane more hydrophilic; that was why hydrophilic property and water uptake of the hybrid membranes enhanced with the increase of $H_6Bi_{12}O_{16}$ (less than 5%). The water content is an important factor affecting the proton conductivity of hybrid membranes, so the variation of proton conductivity is the same as the trend of hydrophilic property and DS15-Bi_{12}-5 has the highest proton conductivity. (II) Moreover, according to the results of IEC test, the added $H_6Bi_{12}O_{16}$ clusters increased the concentration of proton carrier in DS15-Bi_{12}-5 membrane, offering additional proton hopping sites,

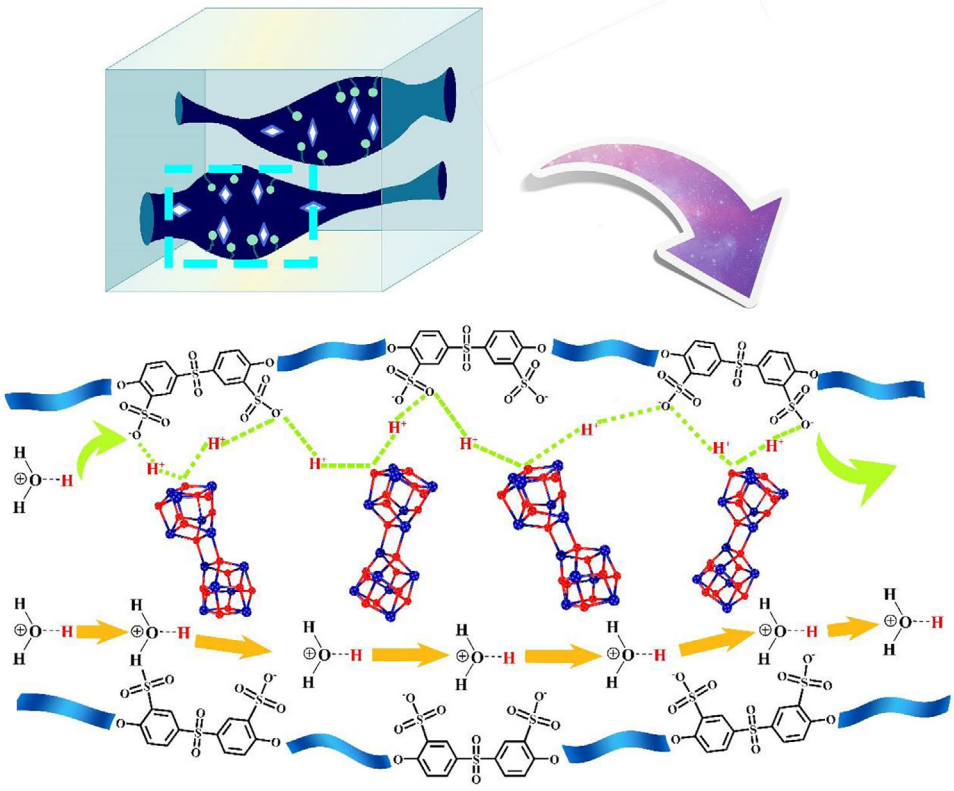

FIGURE 8 Possible proton conduction mechanism in hybrid membranes. The upper dash light blue box is hydrophilic ion domain in the hybrid membranes. The light green arrow indicates the proton transfer pathway under Grotthuss mechanism. The yellow arrow indicates the proton transfer pathway under Vehicle mechanism

further arousing the faster proton transportation. The two factors mentioned above played a dominant role at lower doping content. When the doping amount exceeded 5 wt%, too much fillers occupied the gap between the polymer chains and hindered the normal interactions between $H_6Bi_{12}O_{16}$ clusters and -SO_3H groups, leading to a decrease in hydrophilic property, water uptake, and proton conductivity. The presumed mechanism of protons transport in hybrid membranes was shown in Figure 8.

2.7 | Methanol permeability and relative selectivity

Methanol crossover has been measured to evaluate the usability of the membranes for PEMFCs. The methanol permeability of DS15-Bi_{12}-0 and DS15-Bi_{12}-5 are 1.76×10^{-10} and 1.57×10^{-10} $cm^2 \cdot s^{-1}$, respectively. This extraordinary methanol barrier performance can be attributed to the low degree of sulfonation of our SPEAKS membrane. Furthermore, the methanol permeability of DS15-Bi_{12}-5 was lower than the pure SPAEKS membrane, proving that the introduction of $H_6Bi_{12}O_{16}$ had a positive effect in enhancing the fuel barrier capacity of SPAEKS. The continuous network of hydrogen bonds between $H_6Bi_{12}O_{16}$ clusters and -SO_3H groups could effectively hinder the methanol crossover and with proper increases of fillers content, the dense cluster structure of POM could further obstruct the pass of methanol molecules. This result is consistent with the conclusion in the previous literature. The selectivity (β) of DS15-Bi_{12}-0 and DS15-Bi_{12}-5 are 0.906×10^{-8} and 1.93×10^{-8} $S \cdot s \cdot cm^{-3}$, respectively. The selectivity of hybrid membrane has been obviously increased owing to the enhanced proton conductivity and the decreased methanol permeability. These results further proved the significance of doping POMs to SPAEKS with low sulfonation degree.

2.8 | The chemical stability of the membranes

As shown in Table S1, the residual weight ratio of prepared membranes ranged from 99.34% to 98.18%. This result showed that the oxidation stability of all these SPAEKS membranes are very high owing to relative low degree of sulfonation, which lead to less possibility of being attack by free radicals. The oxidation stability of DS15-Bi_{12}-5 is 98.18%. It means that the hydrophilic regions of DS15-Bi_{12}-5 can almost remain intact after being attacked by free radicals, proving its great potential in practical application.

3 | CONCLUSION

In conclusion, we synthesized a series of high performance PEMs by doping high positive charge $H_6Bi_{12}O_{16}$ clusters into low-sulfonated SPAEKS. Specifically, DS15-Bi_{12}-5 exhibited the best proton conductivity of 72.8 mS·cm^{-1} at 80°C and the tensile strength increased to a level of 43.57 MPa. After the incorporation of Bi clusters, continuous network of hydrogen bonds had been fabricated. Further, the added $H_6Bi_{12}O_{16}$ clusters offered additional proton hopping sites and increased the concentration of proton carriers. In this way, the processes of Grotthuss mechanism and vehicle mechanism are both promoted, resulting in high proton conductivity. The existence of POMs and the increased hydrogen bond networks also reinforced the interactions within the polymer, leading to an improvement in mechanical properties, making

g these hybrid membranes more competitive in practical use. This strategy reveals the potential possibility of POMs as a substitute for sulfonate in PEMs and opens up a broad prospect for the design of low-sulfonated SPAEKS for the application in PEMs.

4 | EXPERIMENTAL SECTION

4.1 | Chemicals

4,4′-difluorobenzophenone (99% purity), N-methyl-2-pyrrolidinone (NMP, AR grade), sulfolane (AR grade), bisphenol A (AR grade), 4,4′-dichlorodiphenylsulfone (AR grade), and bismuth nitrate pentahydrate (99.0% purity) were purchased from Shanghai Macklin Biochemical Industry Park. K_2CO_3 (AR grade) was purchased from Fuchen (Tianjin) Chemical Reagents Co., Ltd. Toluene (AR grade) was purchased from Tianjin Fuyu Fine Chemical Co., Ltd. Nitric acid was obtained from Xilong Scientific Co., Ltd.

4.2 | Synthesis of $H_6Bi_{12}O_{16}$ clusters

$H_6Bi_{12}O_{16}$ clusters were synthesized according to the previous literature.[35] $Bi(NO_3)_3{\cdot}5H_2O$ (5 g, 0.01 mol) was dispersed in 5 ml HNO_3 (65%) with stirring, and the mixture was diluted to 500 ml with deionized water. The solution was treated under ultrasonic for 30 min at room temperature. Four percent NaOH solution was used to adjust the pH value of the mixed solution to 1.5 and the nanocrystals of $H_6Bi_{12}O_{16}$ clusters were obtained. After filtration, the precipitates were washed with deionized water and collected after drying.

4.3 | Synthesis of 3,3′-disulfonated-4,4′-dichlorodiphenyl sulfone (SDCDPS)

The monomer was synthesized according to the method reported by Chen and Awasthi; some modifications had been added.[36,37] 4,4′-dichlorodiphenylsulfone (14.358 g, 50 mmol) and 30 ml fuming sulfuric acid (20% SO_3) were placed in a round bottom flask and the solution was stirred at 40°C to dissolve; an amber homogeneous transparent solution was obtained. The mixture was slowly heated to 110°C and held at this temperature for 10 h. After heating, the mixture was cooled down to room temperature and 370 ml ice water was added. NaOH was added to neutralize the excess fuming sulfuric acid, making the pH value of the mixture reach to 8. NaCl was slowly added until the light yellow transparent solution became turbid. A large amount of white solid precipitation was obtained. White needle crystals were obtained after recrystallization. The solid was filtered and dried at 60°C for 48 h.

4.4 | Synthesis of SPAEKS

SPAEKS was prepared according to previous report.[38,39] In order to avoid the oxidation of bisphenol A, solid chemicals were dried overnight in a vacuum oven at 60°C. 4,4′-difluorobenzophenone (4.0367 g, 0.0185 mol), SDCDPS (0.7369 g, 0.0015 mol), bisphenol A (4.5658 g, 0.02 mol), and anhydrous K_2CO_3 (5.5284 g, 0.04 mol) were put in a three-necked flask, equipped with a mechanical stirrer. Twenty-one milliliters of sulfolane and 18 ml toluene were added into the three-necked flask. The mixture was fully stirred for 0.5 h. Then, the temperature was raised to 126°C slowly (about 10°C/20 min). The reaction mixture was stirred and refluxed at 126°C for 4 h. After that, toluene was discharged. Then the reaction temperature was gradually increased to 190°C. Five hours later, the reaction system reached a certain viscosity, and then the viscous mixture was poured into water a little bit slowly to get cooled copolymer. The surface of the polymer was cleaned with deionized water. The product was cut into small segments and boiled with deionized water three times to remove impurities. Finally, SPAEKS was dried in oven at 70°C.

4.5 | Preparation of hybrid membranes

The $H_6Bi_{12}O_{16}$-doped hybrid SPAEKS membranes were prepared by solution casting method and the doping amount was determined by the mass fraction of $H_6Bi_{12}O_{16}$. Dried SPAEKS (0.27 g) and $H_6Bi_{12}O_{16}$ clusters (0.0081–0.054 g; for DS15-Bi_{12}-0,; $H_6Bi_{12}O_{16}$ clusters was

not added) were dissolved in 5.8 g NMP. The mixture was stirred for 12 h and treated under ultrasonic for another 1 h, obtaining a light yellow even translucent casting mixture (for DS15-Bi_{12}-0, the casting mixture is completely transparent). The obtained solution was uniformly poured onto glass plate and dried at 70°C for 48 h. Hybrid membranes DS15-Bi_{12}-0, DS15-Bi_{12}-3, DS15-Bi_{12}-5, DS15-Bi_{12}-10, DS15-Bi_{12}-15, and DS15-Bi_{12}-20 were obtained (DS = 15%, Bi_{12} is short for $H_6Bi_{12}O_{16}$, and the doping amount of $H_6Bi_{12}O_{16}$ is from 0 wt% to 20 wt%). The thickness of the prepared polymer membrane was about 30 μm.

4.6 | Characterization and instruments

SEM (JEOL, JMS-7610F, Japan) was used to observe cross-section morphology of SPAEKS membrane and $H_6Bi_{12}O_{16}$-doped hybrid SPAEKS membranes. PXRD was performed on Rigaku/Smarlab. The FT-IR (Thermo Fisher Nicolet) was used to perform the structure of $H_6Bi_{12}O_{16}$ clusters, SPAEKS membrane, and hybrid membranes. The thermal stabilities were performed through Pyris 1TGA, PerkinElmer. The ^{1}H NMR spectrum of SPAEKS was recorded on 400 MHz Bruker Avance III spectrometer using DMSO-d_6 as solvent. The impedance was measured by Biological SP-300.

4.7 | Water uptake and swelling ratio measurement

Water uptake and swelling ratio of SPAEKS membrane and $H_6Bi_{12}O_{16}$-doped hybrid SPAEKS membranes were studied by the method similar to previous literature.[40] The formulas were as follows:

$$\text{Water uptake } (\%) = \left[\left(W_{\text{wet}} - W_{\text{dry}}\right)/W_{\text{dry}}\right] \times 100\%, \quad (1)$$

$$\text{Swelling ratio } (\%) = \left[\left(T_{\text{wet}} - T_{\text{dry}}\right)/T_{\text{dry}}\right] \times 100\%. \quad (2)$$

In the above formula, dry and wet represented dry and wet status samples. Where W_{dry}, W_{wet}, T_{dry}, and T_{wet} were weight and thickness of SPAEKS membrane and $H_6Bi_{12}O_{16}$-doped hybrid SPAEKS membranes, respectively.

4.8 | Mechanical properties test

The mechanical properties tests of SPAEKS membrane and $H_6Bi_{12}O_{16}$-doped hybrid SPAEKS membranes were carried out according to the previous literature.[40] The samples were prepared in 50 × 5 mm and immersed in deionized water. The surfaces of these membranes were wiped with filter paper before testing. The rate of extension was 2 mm per minute. The mechanical properties of the hybrid membranes were characterized by tensile strength, elongation-at-break, and Young's modulus.

4.9 | IEC measurement and hydration number (λ)

The IEC of SPAEKS membrane and $H_6Bi_{12}O_{16}$-doped hybrid SPAEKS membranes were measured using the similar method reported in previous literature.[41] First, the samples were immersed in 2 mol·L^{-1} of NaCl aqueous for 48 h to fully exchange H^+. Next, the solution was titrated with NaOH aqueous (0.01 mol·L^{-1}) using phenolphthalein as an indicator. The IEC of SPAEKS membrane and $H_6Bi_{12}O_{16}$-doped hybrid SPAEKS membranes was calculated as follows:

$$\text{IEC} = \left(V_{\text{NaOH}} \times C_{\text{NaOH}}\right)/W_{\text{dry}}, \quad (3)$$

where W_{dry} was the dry weight of the sample, V_{NaOH} was the consumed volume of NaOH, C_{NaOH} was the concentration of NaOH solution.

The hydration number (λ) was calculated according to the following formula[32]:

$$\lambda = (\text{water uptake value}/18.01) \times (10/\text{IEC}), \quad (4)$$

4.10 | Proton conductivity measurement

The proton conductivity of SPAEKS membrane and $H_6Bi_{12}O_{16}$-doped hybrid SPAEKS membranes was measured at different temperature. The impedance of SPAEKS membrane and $H_6Bi_{12}O_{16}$-doped hybrid SPAEKS membranes was measured by four-point-probe AC. During this test, frequency range was 1 Hz–1 MHz.[42,43] Proton conductivities (σ) of SPAEKS membrane and $H_6Bi_{12}O_{16}$-doped hybrid SPAEKS membranes were calculated from formula:

$$\sigma = L/R \cdot d \cdot W, \quad (5)$$

where L (cm) is the distance between two electrodes, R (ohm) is resistance of PEMs, d (cm) is the thickness, and W (cm) is the width of the membrane.

4.11 | E_a calculation

E_a of SPAEKS membrane and $H_6Bi_{12}O_{16}$-doped hybrid SPAEKS membranes was calculated by Arrhenius

equation as follows:

$$\ln(\sigma) = \ln(\sigma_0) - (E_a/RT), \quad (6)$$

where R is 8.314 J·K^{-1}·mol^{-1}, σ_0 is the preexponential factor, T is temperature (K). The E_a can be calculated from the slop of ln[σ/(S·cm^{-1})] vs. 1/T.

4.12 | Methanol permeability

The methanol permeability was tested using the same method reported by previous literature.[34] Two chambers separated by a membrane were saturated with equal amount of deionized water and 10 M methanol solution, respectively. The methanol penetration continued for 2 h under the mechanical stirring. The gas chromatograph (Agilent 6890 N) was used to test the methanol concentration in the water chamber and the methanol permeability of membranes was calculated as below:

$$C_B = (AP/V_B L) C_A T, \quad (7)$$

where A (cm^2) is for the effective area of membranes, P (cm^2·s^{-1}) is the methanol permeability coefficient, C_B (mol·L^{-1}) and C_A (mol·L^{-1}) refer to the methanol concentration in the water chamber and the methanol chamber, respectively. V_B (ml) represents the volume of water or methanol chamber, L (cm) corresponds to the thickness of membranes, T (s) represents the time of methanol permeation.

4.13 | Oxidative stability

It is necessary to test the oxidation stability of SPAEKS and hybrid membranes for the subsequent application of the membrane. We simulated the harsh environment under strong oxidation conditions with Fenton reagent. The dried hybrid membranes were soaked in Fenton's (H_2O_2 solvent of 3% and $FeSO_4$ of 2 ppm) reagents at 80°C for 1 h. The residual masses of the hybrid membranes were recorded to characterize the antioxidant abilities of the hybrid membranes.

ACKNOWLEDGMENTS

This work was financially supported by the National Natural Science Foundation of China (Nos. 21701016 and 51803011), the Science and Technology Development Planning of Jilin Province (No. 20190103129JH), and the Education Department of Jilin Province (No. JJKH20200666KJ). This paper was also supported by the China Scholarship Council (CSC No. 201802335014). Partial support from the Robert A. Welch Foundation (B-0027) (S.M.) is also acknowledged.

CONFLICT OF INTEREST

The authors declare no conflict of interest.

ORCID

Shengqian Ma https://orcid.org/0000-0002-1897-7069

REFERENCES

1. Haseli Y. Maximum conversion efficiency of hydrogen fuel cells. *Int J Hydrogen Energy*. 2018;43:9015-9021.
2. Hooshyari K, Rezania H, Vatanpour V, et al. High temperature membranes based on PBI/sulfonated polyimide and doped-perovskite nanoparticles for PEM fuel cells. *J Membr Sci*. 2020;612:118436.
3. (a) Guo ZM, Chen JN, Byun JJ, et al. High-performance polymer electrolyte membranes incorporated with 2D silica nanosheets in high-temperature proton exchange membrane fuel cells. *J Energy Chem*. 2022;64:323-334. (b) Vinothkannan M, Hariprasad R, Ramakrishnan S, Kim AR, Yoo DJ. Potential bifunctional filler (CeO2 ACNTs) for nafion matrix toward extended electrochemical power density and durability in proton-exchange membrane fuel cells operating at reduced relative humidity. *ACS Sustainable Chem Eng*. 2019;7:12847-12857.
4. Hariprasad R, Vinothkannan M, Kim AR, Yoo DJ. SPVdF-HFP/SGO nanohybrid proton exchange membrane for the applications of direct methanol fuel cells. *J Dispersion Sci Technol*. 2019;42:33-45.
5. Wu L, Zhang Z, Ran J, Zhou D, Li C, Xu T. Advances in proton-exchange membranes for fuel cells: an overview on proton conductive channels (PCCs). *Phys Chem Chem Phys*. 2013;15:4870-4887.
6. (a) Iulianelli A, Basile A. Sulfonated PEEK-based polymers in PEMFC and DMFC applications: a review. *Int J Hydrogen Energy*. 2012;37:15241-15255. (b) Kim AR, Gabunada JC, Yoo DJ. Amelioration in physicochemical properties and single cell performance of sulfonated poly(ether ether ketone) block copolymer composite membrane using sulfonated carbon nanotubes for intermediate humidity fuel cells. *Int J Energy Res*. 2019;43:2974-2989.
7. He C, Mighri F, Guiver MD, Kaliaguine S. Tuning surface hydrophilicity/hydrophobicity of hydrocarbon proton exchange membranes (PEMs). *J Colloid Interface Sci*. 2016;466:168-177.
8. (a) Li HQ, Liu XJ, Xu JM, et al. Enhanced proton conductivity of sulfonated poly(arylene ether ketone sulfone) for fuel cells by grafting triazole groups onto polymer chains. *J Membr Sci*. 2016;509:173-181. (b) Xu JM, Zhang ZG, Yang K, Zhang HX, Wang Z. Synthesis and properties of novel cross-linked composite sulfonated poly (aryl ether ketone sulfone) containing multiple sulfonic side chains for high-performance proton exchange membranes. *Renew Energ*. 2019;138:1104-1113. (c) Lee KH, Chu JY, Mohanraj V, Kim AR, Song MH, Yoo DJ. Enhanced ion conductivity of sulfonated poly(arylene ether sulfone) block copolymers linked by aliphatic chains constructing wide-range ion cluster for proton conducting electrolytes. *Int J Hydrogen Energy*. 2020;45:29297-29307.

9. Vinothkannan M, Kannan R, Kim AR, Kumar GG, Nahm KS, Yoo DJ. Facile enhancement in proton conductivity of sulfonated poly (ether ether ketone) using functionalized graphene oxide synthesis, characterization, and application towards proton exchange membrane fuel cells. *Colloid Polym Sci*. 2016;294:1197-1207.
10. (a) Wu W, Li Y, Liu J, et al. Molecular level hybridization of nafion with quantum dots for highly enhanced proton conduction. *Adv Mater*. 2018;30:1707516. (b) Sigwadi R, Mokrani T, Dhlamini S, Msomi PF. Nafion reinforced with polyacrylonitrile/ZrO2 nanofibers for direct methanol fuel cell application. *J Appl Polym Sci*. 2020;138:49978.
11. Sivasubramanian G, Gurusamy Thangavelu SA, Maria Mahimai B, Hariharasubramanian K, Deivanayagam P. Unprecedented sulphonated poly(ether ether ketone) bismuth cobalt zinc oxide composites: physicochemical and electrochemical performance in fuel cell. *J Mater Sci: Mater Electron*. 2021. https://doi.org/10.1007/s10854-021-06672-1.
12. Wang YY, Shen HC, Cui CF, et al. Towards to better permeability and antifouling sulfonated poly (aryl ether ketone sulfone) with carboxyl group ultrafiltration membrane blending with amine functionalization of SBA-15. *Sep Purif Technol*. 2021;265:118512.
13. Das P, Mandal B, Gumma S. L-tyrosine grafted palladium graphite oxide and sulfonated poly(ether ether ketone) based novel composite membrane for direct methanol fuel cell. *Chem Eng J*. 2021;423:130235.
14. Li JS, Lou JQ, Wang Z, et al. Facilitating proton transport with enhanced water conservation membranes for direct methanol fuel cells. *ACS Sustainable Chem Eng*. 2020;8:5880-5890.
15. Meng XY, Song K, Lv Y, et al. SPEEK proton exchange membrane with enhanced proton conductivity stability from phosphotungstic acid-encapsulated silica nanorods. *Mater Chem Phys*. 2021;272:125045.
16. Oh K, Son B, Sanetuntikul J, Shanmugam S. Polyoxometalate decorated graphene oxide/sulfonated poly(arylene ether ketone) block copolymer composite membrane for proton exchange membrane fuel cell operating under low relative humidity. *J Membr Sci*. 2017;541:386-392.
17. Sun ML, Wang YR, He WW, et al. Efficient electron transfer from electron sponge polyoxometalate to single metal site metal organic frameworks for highly selective electroreduction of carbon dioxide. *Small*. 2021;17:2100762.
18. Pow RW, Sinclair ZL, Bell NL, et al. Enantioselective recognition of racemic amino alcohols in aqueous solution by chiral metal oxide keplerate {Mo 132 } cluster capsules. *Chem Eur J*. 2021;27:12327-12334.
19. Traustason H, Bell NL, Caranto K, et al. Reactivity, formation, and solubility of polyoxometalates probed by calorimetry. *J Am Chem Soc*. 2020;142:20463-20469.
20. Garrido Ribo E, Bell NL, Xuan W, et al. Synthesis, assembly, and sizing of neutral, lanthanide substituted molybdenum blue wheels {Mo 90 Ln 10 }. *J Am Chem Soc*. 2020;142:17508-17514.
21. Müller A, Krickemeyer E, Bögge H, Schmidtmann M, Peters F. Organizational forms of matter: an inorganic super fullerene and keplerate based on molybdenum oxide. *Angew Chem Int Ed*. 1998;37:3360-3363.
22. Rodriguez-Albelo LM, Ruiz-Salvador AR, Sampieri A, et al. Zeolitic polyoxometalate-based metal organic frameworks (Z-POMOFs): computational evaluation of hypothetical polymorphs and the successful targeted synthesis of the redox-active Z-POMOF1. *J Am Chem Soc*. 2009;131:16078-16087.
23. Liu WJ, Dong LZ, Li RH, et al. Different protonic species affecting proton conductivity in hollow spherelike polyoxometalates. *ACS Appl Mater Interfaces*. 2019;11:7030-7036.
24. Li SJ, Zhao Y, Knoll S, et al. High proton conductivity in covalently linked polyoxometalate organoboronic acid polymers. *Angew Chem Int Ed*. 2021;60:16953-16957. *Angew. Chem*. **2021**, *133*, 17090-17094.
25. Gao ZX, Sun S, Li B, et al. Design and synthesis of phosphomolybdate coordination compounds based on {P4Mo6} structural units and their proton conductivity. *Tungsten*. 2021. https://doi.org/10.1007/s42864-021-00122-5.
26. Lee KH, Chu JY, Kim AR, Nahm KS, Kim CJ, Yoo DJ. Densely sulfonated block copolymer composite membranes containing phosphotungstic acid for fuel cellmembranes. *J Membr Sci*. 2013;434:35-43.
27. Yin YH, Li HB, Wu H, Wang W, Jiang ZY. Enhancement in proton conductivity by blending poly(polyoxometalate)-b-poly(hexanoic acid) block copolymers with sulfonated polysulfone. *Int J Hydrogen Energy*. 2020;45:15495-15506.
28. Wu H, Wu XF, Wu QY, Yan WF. High performance proton-conducting composite based on vanadium-substituted Dawson-type heteropoly acid for proton exchange membranes. *Compos Sci Technol*. 2018;162:1-6.
29. Zhai L, Li H. Polyoxometalate polymer hybrid materials as proton exchange membranes for fuel cell applications. *Molecules*. 2019;24:3425.
30. Ogiwara N, Tomoda M, Miyazaki S, et al. Integrating molecular design and crystal engineering approaches in non-humidified intermediate-temperature proton conductors based on a Dawson-type polyoxometalate and poly(ethylene glycol) derivatives. *Nanoscale*. 2021;13:8049-8057.
31. Liu YW, Liu SM, Lai XY, et al. Polyoxometalate-modified sponge-like graphene oxide monolith with high proton-conducting performance. *Adv Funct Mater*. 2015;25:4480-4485.
32. Kim AR, Vinothkannan M, Kim JS, Yoo DJ. Proton-conducting phosphotungstic acid/sulfonated fluorinated block copolymer composite membrane for polymer electrolyte fuel cells with reduced hydrogen permeability. *Polym Bull*. 2017;75:2779-2804.
33. (a) Liu BL, Cheng DM, Zhu HT, et al. A bismuth oxide/graphene oxide nanocomposite membrane showing super proton conductivity and low methanol permeability. *Chem Sci*. 2019;10:556-563. (b) Liu B, Hu B, Du J, et al. Precise molecular-level modification of Nafion with bismuth oxide clusters for high-performance proton exchange membranes. *Angew Chem Int Ed*. 2021;60:6076-6085; *Angew Chem.* 2021, *133*, 6141-6150.
34. Li JS, Wang S, Xu JM, et al. Organic-inorganic composite membrane based on sulfonated poly (arylene ether ketone sulfone) with excellent long-term stability for proton exchange membrane fuel cells. *J Membr Sci*. 2017;529:243-251.
35. Lazarini F. The crystal structure of a bismuth basic nitrate, [Bi6O5(OH)3](NO3)5.3H2O. *Acta Cryst*. 1978;B34:3169.
36. Wang F, Chen TL, Xu JP. Sodium sulfonate-functionalized poly(ether ether ketone)s. *Macromol Chem Phys*. 1998;199:1421-1426.
37. Awasthi S, Kiran V, Gaur B. Crosslinked poly(ether ether ketone): cost-effective proton exchange membranes for fuel cell application. *Bull Mater Sci*. 2018;41:9.

38. Xu LS, Xu JM, Liu MY, et al. Fabrication of sulfonated poly(aryl ether ketone sulfone) membranes blended with phosphotungstic acid and microporous poly(vinylidene fluoride) as a depository for direct-methanol fuel cells. *Int J Hydrogen Energy*. 2015;40:7182-7191.
39. Yang K, Ni HZ, Du XM, et al. Improvement the hydroxide conductivity and alkaline stability simultaneously of anion exchange membranes by changing quaternary ammonium and imidazole contents. *Int J Energy Res*. 2021;45:13668-13680.
40. Xu JM, Zhang ZG, Yang K, et al. Construction of new transport channels by blending POM-based inorganic-organic complex into sulfonated poly(ether ketone sulfone) for proton exchange membrane fuel cells. *J Membr Sci*. 2020;596:117711.
41. Zhang ZG, Ren JH, Xu JM, Meng LX, Zhao PY, Wang Z. Long-term durable solid state electrolyte membranes based on a metal organic framework with phosphotungstic acid confined in the mesoporous cages. *Int J Hydrogen Energy*. 2020;45:27527-27538.
42. Zhang Z, Ren J, Xu J, et al. Adjust the arrangement of imidazole on the metal-organic framework to obtain hybrid proton exchange membrane with long-term stable high proton conductivity. *J Membr Sci*. 2020;607:118194.
43. Liu F, Wang S, Chen H, et al. Cross-linkable polymeric ionic liquid improve phosphoric acid retention and long-term conductivity stability in polybenzimidazole based PEMs. *ACS Sustainable Chem Eng*. 2018;6:16352-16362.

SUPPORTING INFORMATION

Additional supporting information may be found in the online version of the article at the publisher's website.

How to cite this article: Yin Yi-Z, Zhang Z-G, He W-W, et al. Precise modification of poly(aryl ether ketone sulfone) proton exchange membranes with positively charged bismuth oxide clusters for high proton conduction performance. *SusMat*. 2022;2:76–89. https://doi.org/10.1002/sus2.41